POLITECNICO
MILANO 1863

SCUOLA DI INGEGNERIA INDUSTRIALE
E DELL'INFORMAZIONE

EXECUTIVE SUMMARY OF THE THESIS

Synthesis and development of a phototunable MeHA-based 3D *in vitro* model of wound healing and fibrosis

TESI MAGISTRALE IN BIOMEDICAL ENGINEERING – INGEGNERIA BIOMEDICA

AUTHOR: JACOPO CERVILLIO

ADVISOR: PROF. EMANUELA JACCHETTI

CO-ADVISOR: PROF. MARK W. TIBBITT, DR. JAIMIE MAYNER

ACADEMIC YEAR: 2024-2025

1 Introduction

Wound healing is a tightly regulated process that restores tissue integrity after injury through coordinated interactions between immune cells, stromal cells and the extracellular matrix (ECM). When repair fails to resolve, it can progress toward fibrosis, a pathological state characterized by persistent inflammation, excessive ECM deposition, myofibroblast accumulation and progressive tissue stiffening, that compromises functional recovery. Fibrotic remodeling represents a major clinical problem across multiple organs, including skin, lung, heart and liver, highlighting the broad relevance of understanding how physiological repair transitions into pathological scarring.

A central aspect of wound healing is the time-dependent evolution of the mechanical microenvironment. Beyond biochemical signaling, mechanical cues actively regulate cellular behavior through mechanotransduction: cells sense ECM stiffness and architecture via integrin-mediated adhesions coupled to the cytoskeleton, transmitting forces to intracellular signaling pathways and the nucleus.

ECM stiffening during wound healing and its further increase in fibrosis modulates fibroblasts and macrophages behavior. Fibroblasts remodel the matrix by differentiating into contractile myofibroblasts that generate tensile forces and deposit new ECM, reinforcing tissue stiffening. Macrophages integrate inflammatory and mechanical signals and promote fibroblast activation through factors such as TGF-β. Their bidirectional crosstalk couples immune signaling to mechanical feedback and determines whether healing resolves or progresses toward fibrosis.

In vitro models are essential to investigate these cellular and molecular mechanisms under controlled conditions. While two-dimensional systems have provided important mechanistic insights, they fail to reproduce three-dimensional architecture and physiologically relevant force

transmission. Hydrogel-based three-dimensional models provide improved control over matrix composition and stiffness, enabling more representative cell-cell and cell-ECM interactions; however, many conventional hydrogels form dense nanoporous networks that physically confine cells and limit nutrients diffusion, cell spreading and migration.

To address these limitations, this thesis develops a phototunable three-dimensional methacrylated hyaluronic acid (MeHA) granular hydrogel platform. By combining dynamic control of stiffness with a macroporous granular architecture, the system enables investigation of how static and time-dependent mechanical cues regulate fibroblast behavior and immune-stromal interactions in wound healing and fibrosis. Although dermal mechanics are used to define physiologically relevant stiffness targets, the platform is conceptually adaptable to other fibrotic tissues by redefining mechanical ranges and incorporating tissue-relevant cell populations, providing a versatile framework for studying mechanobiology across different organs.

2 Materials and Methods

2.1 MeHA synthesis

The synthesis of methacrylated hyaluronic acid (MeHA) was adapted from a previously developed protocol from Burdick *et al.* [1]. Sodium hyaluronate (60 kDa HA) was dissolved in Milli-Q water at 2 % w/v under overnight stirring. The solution pH was adjusted to 8 with 1 M NaOH prior to the dropwise addition of methacrylic anhydride (5.6 mL/g HA) under stirring in an ice bath (1 mL of MA every 20-30 minutes). During the reaction time (8-10 hours), the pH was maintained between 8 and 9 to promote complete functionalization.

The product was purified by centrifugation and dialysis (MWCO 6-8 kDa) against DI water for 7 days, then lyophilized for three days.

MeHA functionalization was quantified by ^{1}H-NMR spectroscopy (Bruker Ascend Aeon 400) by integrating methacrylate vinyl peaks (5.6-5.9 ppm and 6.1-6.4 ppm) and normalizing them to the HA backbone signals (3.0-4.6 ppm) using MestReNova. To reduce batch-to-batch variability, multiple batches were pooled, re-dialyzed, sterile-filtered, frozen, lyophilized and stored at -80 °C until use.

2.2 Hydrogel fabrication and rheological characterization

2.2.1 Bulk hydrogels

Bulk MeHA hydrogels were formed via Michael-type addition between methacrylate groups on MeHA and $PEG(SH)_2$, following the strategy described by Caliari *et al.* [2]. MeHA (60 mg/mL in PBS) was mixed with RGD peptide and triethanolamine buffer prior to addition of $PEG(SH)_2$. Thiol to methacrylate ratios ranging from 1:10 to 1:1 were used to modulate initial crosslinking density and obtain different stiffnesses. Hydrogels were cast between spacer-defined glass coverslips (500 μm), allowed to crosslink for 2 hours at room temperature and swollen overnight in PBS at 4°C.

To enable dynamic stiffening, a secondary photoinitiated free-radical polymerization step was performed: swollen hydrogels were incubated in LAP solution and exposed to 405 nm light (10 mW/cm^2, 10 minutes) to polymerize residual methacrylate groups, thereby increasing network crosslink density and hydrogel stiffness.

2.2.2 Granular hydrogels

Granular hydrogels were generated by mechanically fragmenting bulk hydrogels using a syringe-based sieving approach adapted from Kessel *et al.* [3]. Bulk hydrogels were passed three times through a 90 μm mesh to produce microgel fragments. Granular hydrogels were swollen in growth medium and stored at 4 °C.

2.2.3 Rheological characterization

Bulk and granular hydrogels were characterized using a rheometer (Anton Paar MCR 502) equipped with an 8 mm sandblasted parallel-plate geometry. Oscillatory measurements were performed at 37 °C using time sweeps at constant strain amplitude $\gamma = 0.5\%$ and angular frequency $\omega = 1$ rad/s to determine storage modulus (G′) and loss modulus (G″). Granular suspensions were centrifuged to obtain a jammed phase and remove excess medium prior to measurements.

For *in situ* stiffening measurements, the rheometer was equipped with a custom glass stage enabling illumination from below. Rheological measurements were performed before, during (405 nm, 10 mW/cm^2 for 10 minutes) and after light-induced secondary crosslinking.

G′ and G″ values recorded by the rheometer were averaged over the plateau region of each measurement and plotted in GraphPad Prism for comparison across formulations.

2.3 Microfluidic device fabrication

PDMS microfluidic devices were fabricated by soft lithography using master molds developed by Krattiger *et al.* [4] (Figure 1). PDMS base and curing agent were mixed (9:1 w/w ratio), cast on the master mold, degassed and cured at 70 °C for 1 hour. Devices were punched for inlets/outlets and oxygen plasma bonded to glass coverslips (#1.5), followed by baking at 80 °C for 1 hour. Devices were sterilized prior to cell experiments.

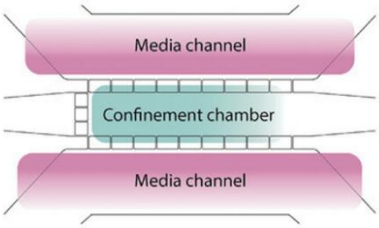

Figure 1: Schematic of the microfluidic device layout with a central confinement chamber and two adjacent media channels. The confinement chamber is 1 mm wide and uses 490 μm-long pillars with 30 μm spacing [4].

2.4 Co-loading of granular hydrogels and cells in a microfluidic device

Granular MeHA hydrogels were co-loaded with neonatal human dermal fibroblasts (NHDF) into microfluidic devices to immobilize the hydrogel network and establish a three-dimensional culture environment compatible with fluorescence imaging. NHDF were cultured in DMEM supplemented with 10% FBS and 1% penicillin-streptomycin at 37 °C and 5% CO_2.

Prior to loading, microgels were centrifuged to obtain a jammed phase and mixed with cells in the presence of methylcellulose to increase viscosity. The cell-hydrogel suspension was introduced into the confinement chamber and channel filling was visually confirmed by microscopy. After 24 hours of culture, samples were fixed (4% PFA), permeabilized (Triton X-100) and stained for F-actin (phalloidin) and nuclei (DAPI). Fluorescence microscopy (THUNDER Imager Cell microscope) was used to visualize cell distribution and cytoskeletal organization within the three-dimensional granular matrix. Image visualization and processing were performed using Fiji (ImageJ), including z-stack reconstruction and maximum intensity projections.

2.5 Monocyte isolation from whole blood

PBMCs were isolated from residual donor whole blood by Ficoll-Paque density-gradient centrifugation. Monocytes were enriched by negative immunomagnetic selection (StemCell Technologies), enabling isolation of untouched primary monocytes while minimizing activation.

Monocyte purity was confirmed by flow cytometry using viability staining and lineage-associated surface markers (CD14 and CD16). Data acquisition was performed using a spectral cytometer (Cytek Aurora) and analysis was conducted in FlowJo using consistent gating strategies across experiments.

3 Results and Discussion

3.1 MeHA synthesis

Methacrylated hyaluronic acid was synthesized to obtain a highly functionalized polymer suitable for covalent hydrogel crosslinking. The goal was to achieve a high degree of methacrylation (near-complete substitution of primary hydroxyl groups) in order to maximize the density of polymerizable methacrylate groups and enable both primary network formation and subsequent photo-stiffening.

Initial synthesis attempts resulted in low and poorly reproducible degrees of functionalization, as determined by ^{1}H NMR analysis. The protocol was therefore optimized by adjusting parameters known to influence HA functionalization efficiency: controlled cooling, improved pH control and gradual methacrylic anhydride addition were implemented to improve reaction consistency and limit undesired side reactions (*e.g.* methacrylic anhydride hydrolysis).

Following optimization, reproducible MeHA batches exhibiting high functionalization were obtained. Figure 2 shows a representative ^{1}H NMR spectrum of the final MeHA product. The presence of characteristic vinyl proton peaks at approximately 5.6-6.1 ppm confirms successful

methacrylation, while integration relative to HA backbone signals is consistent with a high functionalization degree suitable for the targeted crosslinking requirements.

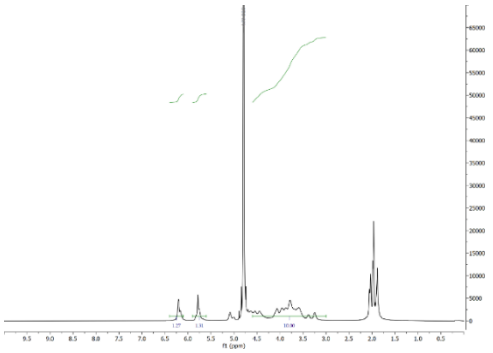

Figure 2: ^{1}H NMR spectrum of MeHA. Vinyl proton peaks at 5.6-6.1 ppm indicate successful functionalization of the HA backbone. Integration of vinyl peaks relative to HA backbone resonances (3.0-4.6 ppm) yielded an estimated degree of methacrylation of ~130% (MestReNova), interpreted as a near-complete methacrylation (analytical overestimation).

The optimized procedure was adopted to produce ~10 g of MeHA which was subsequently pooled to minimize batch-to-batch variability and provide a uniform starting material for hydrogel fabrication.

3.2 Hydrogel fabrication and characterization

3.2.1 Bulk hydrogels

Bulk MeHA hydrogels were fabricated via Michael-type addition using $PEG(SH)_2$ as a dithiol linker. Hydrogel stiffness was tuned by varying the thiol to methacrylate ratio from 1:10 to 1:1, with higher $PEG(SH)_2$ content producing stiffer networks. Across formulations, rheology showed a wide stiffness window (G′ ≈ 0.28-37.59 kPa) and a consistent monotonic increase in G′ with increasing linker content (Figure 3).

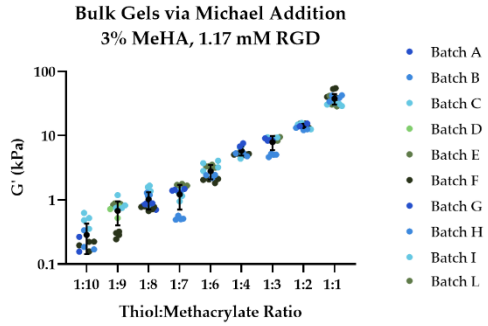

Figure 3: Bulk MeHA hydrogel stiffness (G′) as a function of thiol:methacrylate ratio. Colored points: individual rheology measurements color-coded by batch (n = 4 batches per formulation; n = 5 for 1:8 formulation). Black points: mean G′ for each formulation and error bars indicating the standard deviation calculated across all measurements pooled within that formulation.

To define dermis-relevant mechanical targets, literature values were used, acknowledging that reported skin stiffness depends strongly on anatomical site, dermal layer and measurement method. Importantly, dermal stiffness is commonly reported in literature as elastic modulus (E), whereas rheological measurements provide the shear modulus (G). Assuming nearly incompressible hydrogels ($\nu \approx 0.5$), $E \approx 3G$; here, the shear modulus G was approximated as G′ because oscillatory measurements consistently showed G′ >> G″ under the selected conditions. Using this mapping, ~3 kPa (E) was used as a representative healthy dermis reference and ~10-30 kPa (E) as a fibrotic range, guiding the selection of "soft" and "stiff" hydrogel formulations and dynamic soft-to-stiff trajectories.

Time-dependent mechanics were implemented by exploiting residual methacrylate groups for secondary photo-crosslinking via LAP-initiated free-radical polymerization under 405 nm illumination. With 0.1% LAP, all tested formulations exhibited increased G′ after light exposure; notably, soft starting conditions (1:9 and 1:8) could be stiffened into the range of a static stiff condition (1:4), demonstrating feasibility of mechanically distinct static and dynamic states (Figure 4).

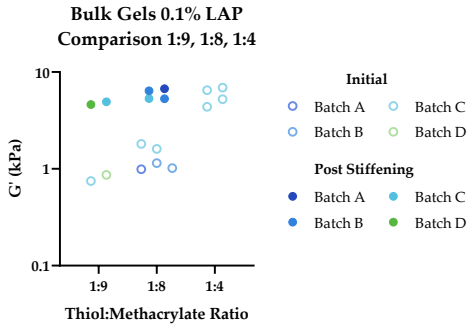

Figure 4: Comparison of selected bulk formulations stiffened with 0.1% (w/v) LAP. Storage modulus (G′) is shown before (non-filled circles) and after stiffening (filled circles). Colors denote independent batches. Softer starting formulations (1:9, 1:8) reached post-stiffening values approaching the static stiffness range of the stiffer 1:4 formulation.

To move toward more cell-compatible and temporally controlled stiffening, *in situ* stiffening was also evaluated using 0.01% LAP. At this lower initiator concentration, stiffness increases were smaller per exposure, but sequential irradiation enabled soft formulations (1:9, 1:7, 1:6) to approach the target stiff range (1:4) while extending the stiffening timeline (Figure 5).

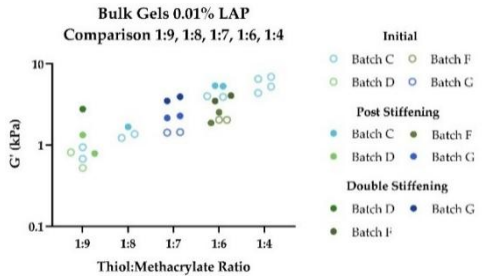

Figure 5: Comparison of selected bulk formulations stiffened with 0.01% (w/v) LAP. Storage modulus (G′) is shown before irradiation (non-filled circles), after a single stiffening step (light filled circles) and after double stiffening (dark filled circles). Colors denote independent batches. Lower initiator concentration produced smaller stiffness increases per exposure, while sequential irradiation improved access to the target stiffness range of the 1:4 formulation.

Together, these results establish two usable stiffening strategies: a robust, faster single-step transition with 0.1% LAP and a more gradual, multi-step, transition with 0.01% LAP, to better approximate progressive stiffening *in vivo*.

3.2.2 Granular hydrogels

To generate a macroporous three-dimensional matrix suitable for cell studies, bulk hydrogels were mechanically fragmented into microgels and assembled into granular networks. Initial rheology of the granular systems showed high variability and a weak dependence on formulation, consistent with the known sensitivity of granular mechanics to jamming state and residual liquid content during sample loading on the instrument. The workflow was therefore refined by standardizing pre-measurement jamming and improving supernatant removal prior to loading.

With these changes, granular measurements recovered a clearer increase in G′ with increasing $PEG(SH)_2$ content and showed reduced inter-batch dispersion, providing a more reliable basis to define "soft" and "stiff" granular conditions for downstream experiments (Figure 6).

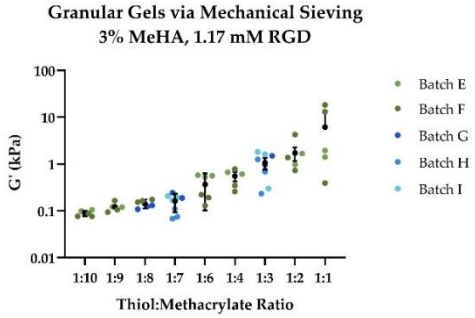

Figure 6: Granular MeHA hydrogels rheology using a refined preparation/loading method. Storage modulus (G′) values are shown for multiple thiol:methacrylate ratios. Colored points: individual rheology measurements. Black points: mean G′ for each formulation with error bars showing ± SD across all measurements pooled within that formulation. Clear stiffness trend with increase in $PEG(SH)_2$ content.

3.3 Co-loading of granular hydrogels and cells in a microfluidic device

Granular MeHA hydrogels (jammed microgel assemblies) were loaded into the confinement chamber of PDMS microfluidic devices to immobilize the three-dimensional matrix during media exchange, fixation and immunostaining, enabling a practical imaging workflow. NHDF were co-loaded with the granular matrix and cultured for 24 hours to assess short-term feasibility of maintaining cells within the chamber and performing fluorescence staining and imaging. The 1:2 formulation was used because it enabled robust loading and retention within the confinement chamber. Brightfield imaging (Figure 7) confirmed a densely packed granular network retained within the chamber. Localized cell aggregates were observed in some regions, which may be attributed to incomplete homogenization of the cell-hydrogel mixture prior to loading.

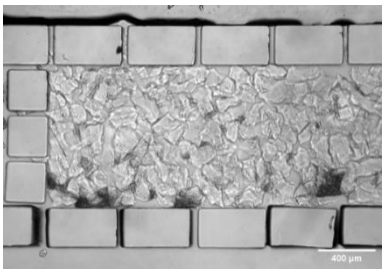

Figure 7: Brightfield images of the microfluidic confinement chamber after co-loading NHDF with a jammed granular MeHA hydrogel (1:2 formulation). The chamber is uniformly filled with a densely packed

granular matrix retained by the pillar array, providing a stable three-dimensional scaffold for subsequent culture, fixation and immunostaining. Scale bar: 400 μm.

Immunostaining for nuclei (DAPI, blue) and F-actin (phalloidin, magenta) was performed to visualize nuclei and cytoskeletal organization across multiple z-planes. Epifluorescence z-stack visualized as maximum intensity projections (MIPs) confirmed the presence of cells throughout the thickness of the granular matrix. Qualitatively, F-actin patterns ranged from perinuclear enrichment (rounded morphology) to more distributed and elongated organization, consistent with cell spreading within the three-dimensional granular matrix (Figure 8). This behavior aligns with the advantage of macroporous architectures where cells reside within interstitial void space, whereas in conventional nanoporous hydrogels cells are embedded within a dense polymer mesh.

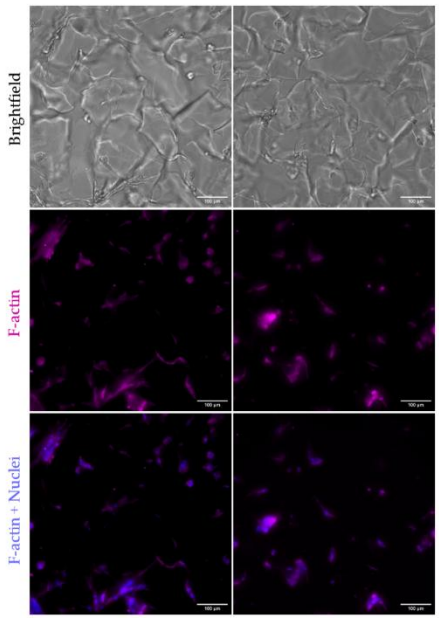

Figure 8: Widefield fluorescence imaging (20× objective) of NHDF within the granular MeHA matrix inside the microfluidic confinement chamber. Brightfield (top), F-actin (phalloidin, magenta; middle) and merged F-actin + nuclei (DAPI, blue; bottom) are shown for two representative regions. Images are maximum-intensity projections from z-stacks (left: 134 μm; right: 161 μm).

Overall, these results demonstrate that the microfluidic device enables retention of the granular matrix during fixation and staining and supports fluorescence imaging throughout the three-dimensional chamber, providing the basis for future comparisons across static soft/stiff conditions and *in situ* stiffening within the device.

3.4 Monocyte isolation from whole blood

Primary human monocytes were isolated from whole blood to support future immune-stromal studies in the platform. Following Ficoll-based PBMC isolation, monocytes were enriched via negative immunomagnetic selection and enrichment was verified by flow cytometry yielding a predominant $CD14^{+}/CD16^{-}$ population consistent with classical monocytes (Figure 9). The workflow was reproducible across independent isolations and aligned with representative profiles reported in literature [5], supporting its suitability as starting point for macrophage differentiation and integration into the mechanically tunable three-dimensional system.

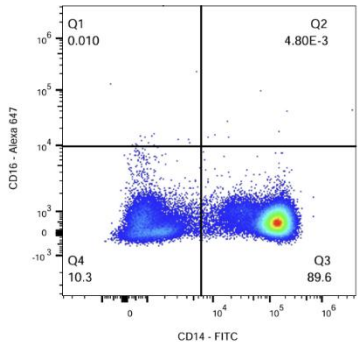

Figure 9: Flow cytometry CD14/CD16 phenotype of isolated primary monocytes after negative immunomagnetic enrichment. Quadrants were set using single-stained compensation bead controls and applied consistently across samples. Within the live singlet gate, the dominant population was $CD14^{+}/CD16^{-}$ (classical monocytes, 89.6%), with a smaller $CD14^{-}/CD16^{-}$ fraction (10.3%); $CD16^{+}$ subsets were negligible.

4 Conclusions and future developments

This work established a reproducible, phototunable three-dimensional hydrogel platform based on methacrylated hyaluronic acid (MeHA) to study mechanobiology in the context of skin wound healing and fibrosis. A robust synthesis protocol was developed to obtain consistent degrees of HA methacrylation across batches, as confirmed by ^{1}H NMR, providing a reliable starting material for reproducible hydrogel fabrication.

Bulk MeHA hydrogels with tunable stiffness were fabricated and macroporous granular matrices

were produced by mechanical fragmentation of bulk gels into microgels. This enabled identification of formulations relevant to physiological and fibrotic stiffness ranges and supported defined mechanical histories, including static soft and stiff states as well as *in situ* photo-stiffening, with tunable kinetics via photoinitiator concentration to better approximate progressive changes *in vivo*.

Granular matrices were integrated into PDMS microfluidic devices to immobilize the jammed microgel network during handling, fixation and immunostaining, enabling three-dimensional imaging workflows. Primary dermal fibroblasts were maintained within the system and displayed organized F-actin structures and cell spreading across multiple z-planes, consistent with cell-matrix interactions within interstitial void space.

Future work should confirm cytocompatibility under the applied photo-stiffening parameters (photoinitiator concentration, light dose, exposure time). In parallel, the relationship between local microgel-scale mechanics and the effective mechanics of the jammed assembly should be quantified, since cellular responses may depend on both.

Moreover, imaging of void space (*e.g.* using FITC-dextran in the aqueous phase) before and after stiffening would further help decouple stiffness-driven effects from geometric and confinement-related contributions.

The next biological objective is to determine how *in situ* dynamic stiffening regulates fibroblast activation over time, with a working hypothesis that it increases cytoskeletal tension and adhesion maturation, promoting a myofibroblast-like phenotype. Readouts should include early mechanotransduction markers and later functional outputs such as α-SMA incorporation into stress fibers and collagen I deposition; transcriptomic profiling (RNA-sequencing) could provide an unbiased route to identify stiffness-responsive programs. Notably, the platform enables three-dimensional culture without collagen as the base polymer, facilitating interpretation of fibroblast-derived collagen deposition as an activation and remodeling readout.

Finally, the monocyte isolation workflow established a foundation for incorporating human immune cells and investigating macrophage-fibroblast crosstalk under defined and evolving mechanical conditions.

Although dermal mechanics guided target selection, the platform can be adapted to other fibrotic tissues by redefining stiffness windows and incorporating tissue-relevant stromal and immune cell populations.

From a translational perspective, identifying mechanistically grounded targets and design rules (*e.g.* stiffness ranges and temporal windows that bias macrophages toward pro-resolving states and limit persistent myofibroblast activation) could inform strategies to reduce pathological scarring and fibrosis, including advanced wound dressings or local biomaterials that modulate inflammatory and mechanical microenvironments. Conversely, defining signaling pathways linked to pro-fibrotic macrophage states may support approaches aimed at interrupting sustained activation loops that reinforce fibrosis.

5 References

[1] J. A. Burdick, C. Chung, X. Jia, M. A. Randolph, and R. Langer, 'Controlled Degradation and Mechanical Behavior of Photopolymerized Hyaluronic Acid Networks', *Biomacromolecules*, vol. 6, no. 1, pp. 386–391, Jan. 2005, doi: 10.1021/bm049508a.

[2] S. R. Caliari *et al.*, 'Stiffening hydrogels for investigating the dynamics of hepatic stellate cell mechanotransduction during myofibroblast activation', *Sci Rep*, vol. 6, no. 1, p. 21387, Feb. 2016, doi: 10.1038/srep21387.

[3] B. Kessel, M. Lee, A. Bonato, Y. Tinguely, E. Tosoratti, and M. Zenobi-Wong, '3D Bioprinting of Macroporous Materials Based on Entangled Hydrogel Microstrands', *Advanced Science*, vol. 7, no. 18, p. 2001419, Sep. 2020, doi: 10.1002/advs.202001419.

[4] L. A. Krattiger *et al.*, 'Microfluidic Platforms to Screen Granular Hydrogel Microenvironments for Tissue Regeneration', *Advanced Functional Materials*, vol. 34, no. 32, p. 2310507, Aug. 2024, doi: 10.1002/adfm.202310507.

[5] M. C. Nielsen, M. N. Andersen, and H. J. Møller, 'Monocyte isolation techniques significantly impact the phenotype of both isolated monocytes and derived macrophages in vitro', *Immunology*, vol. 159, no. 1, pp. 63–74, Jan. 2020, doi: 10.1111/imm.13125.